Transportation Research Part C 142 (2022) 103773

Contents lists available at ScienceDirect

Transportation Research Part C

journal homepage: www.elsevier.com/locate/trc

Modeling and simulation of approaching behaviors to signalized intersections based on risk quantification

Jun Hua [a], Guangquan Lu [a,b,c,*], Henry X. Liu [d,e]

[a] *Beijing Key Laboratory for Cooperative Vehicle Infrastructure System and Safety Control, Beihang University, Beijing 100191, China*
[b] *Beijing Advanced Innovation Center for Big Data and Brain Computing, Beihang University, Beijing 100191, China*
[c] *National Engineering Laboratory for Comprehensive Transportation Big Data Application Technology (NEL-CTBD), Beihang University, Beijing 100191, China*
[d] *Department of Civil and Environmental Engineering, University of Michigan, Ann Arbor, MI 48109, USA*
[e] *University of Michigan Transportation Research Institute (UMTRI), University of Michigan, Ann Arbor, MI 48109, USA*

ARTICLE INFO

Keywords:
Driving behavior model
Signalized intersection
Yellow-light running
Simulation

ABSTRACT

The stop/go decisions made by drivers who are approaching signalized intersections during yellow period will affect the safety and efficiency of intersections. Existing research mostly modeled drivers' decision-making behaviors using real-world driving data, while these datasets were collected in different traffic flows and road environments, and it is difficult to develop models suitable for different intersections. Aiming at explaining the approaching behaviors to signalized intersections from the perspective of human behavioral mechanism, this study establishes a driving behavior model framework, including a risk field model of dynamic traffic control elements independent on yellow duration, and a trajectory planning model constructed according to the risk homeostasis theory and preview-follower theory. Probabilities of passing the stop line during yellow period and the distribution of acceleration and deceleration rates when passing are obtained in the simulation by the Monte Carlo method. Results show the validity of the proposed model and its applicability to drivers with different desired risks. Compared to the proposed model, drivers are more inclined to use smaller acceleration rates or greater deceleration rates when entering intersections in observed cases. The intervention of reaction time may decrease the probabilities of passing. This study is an indispensable supplement to our previous study, contributing a unified model based on risk quantification to comprehensively describe the risk of the traffic environment, and is an attempt to promote the development of driving behavior models.

1. Introduction

Intersections are important nodes in the urban road network, where multiple traffic flows converge. Traffic lights are set to control the stop and go states of vehicles traveling in different directions, thereby maintaining the order of vehicles entering the intersection area. Since the state of traffic lights changes continuously, drivers' decision-making and behaviors at the entrance of a signalized intersection are related to the color change of the traffic light.

When the traffic signal changes from green to yellow, vehicles about to enter the intersection may fall into an area called "dilemma

* Corresponding author.
E-mail address: lugq@buaa.edu.cn (G. Lu).

https://doi.org/10.1016/j.trc.2022.103773
Received 22 October 2021; Received in revised form 13 March 2022; Accepted 22 June 2022
Available online 1 July 2022

zone" (Gazis et al., 1960), where drivers must decide whether to continue going or stop. Whether a vehicle approaching to a signalized intersection will get into the dilemma zone is generally considered to be comprehensively related to vehicle speed, vehicle position at the beginning of the yellow light, and yellow duration (Lu et al., 2015). In the dilemma zone, different decisions made by hesitant drivers will lead to different results. For instance, deciding to continue going may result in red-light-running behaviors and side collisions, while stopping through an emergency brake operation may cause rear-end collisions, and stopping over the stop line tends to obstruct the traffic flows in other directions at the intersection area. Therefore, when the yellow light turns on, approaching behaviors at the entrance of signalized intersections is an important factor affecting the safety and efficiency of the intersections, which has received considerable scholarly attention.

Since a driver's behavior when the yellow light turns on is uncertain, statistical models based on traffic behavior data have advantages in describing drivers' stop/go decisions and behaviors and predicting the possibility of making different decisions. Discrete choice model is usually used to establish the relationship between different decisions taken after the yellow light turns on and different influencing factors, thus to predict the stop/go probability (Papaioannou, 2007; Kim et al, 2008; Pawar et al., 2020). Especially the binary logistic regression model is widely used (Gates and Noyce, 2010; Long et al., 2013; Wu et al., 2018). In addition, fuzzy logic model (Hurwitz et al, 2012; Moore and Hurwitz, 2013; Tang et al, 2016), fuzzy decision tree (Yang et al., 2014), decision tree classification model (Dong and Zhou, 2020), Bayesian network methods (Chen et al., 2018) and agent-based models (Amer et al., 2011; Kim et al., 2016) are also used to describe and predict drivers' decision-making behaviors. Obviously, these models are based on extensive analysis of data, and the factors including vehicle motion status, drivers' individual characteristics and road environmental characteristics that affect decisions and behaviors when the yellow light begins have attracted wide attention from many scholars. According to their findings, the two most important factors are the approach speed and distance to stop line of vehicles at the onset of yellow (Köll et al., 2004; Rakha et al., 2007; Yang et al., 2014; Pathivada and Perumal, 2019), and another variable derived from these two variables, estimated travel time from the start of yellow light to the intersection (Gates et al, 2007), is also one of the key variables. Additionally, some other factors about vehicles have also been found, e.g., acceleration and deceleration when the vehicle approaches (Amer et al., 2011; Sharma et al., 2011), different types of vehicles (Gates and Noyce, 2010), on-board warning systems (Gugerty et al., 2014; Zhang et al., 2021), etc. Moreover, factors related to drivers mainly include age (El-Shawarby et al., 2008; Rakha et al., 2008) and gender (Rakha et al., 2007; Rakha et al., 2008; Li et al., 2020). The influence of distraction has also been studied (Xiong et al., 2016; Savolainen, 2016; Chen et al., 2018; Choudhary and Velaga, 2019). It is worth noting that usually the above two types of factors are related to each other (Chang et al., 1985; Caird et al., 2007). What's more, road environmental factors refer to the characteristics of intersections (Pathivada and Perumal, 2019) and traffic lights (Gates et al, 2007; Kim et al., 2008; Long et al., 2013; Yang et al., 2014; Savolainen, 2016). In summary, these studies are data-driven and can provide references for drivers making macro-decisions and the improvement of traffic facilities. However, without considering the link of risk perception, these studies only looked for some behavioral rules emerging from considerable data to predict the possibility of making different decisions, which were not carried out from the human behavioral mechanism and could not further represent movement trajectories of vehicles from a micro-operational level.

Many scholars used some quantitative indicators to describe the driving risk and took them as the judgment basis of vehicle motion decisions. For instance, in car-following and lane-changing scenarios, longitudinal distances such as gap distance and DHW (distance headway) involving adjacent vehicles are used as evaluation indicators (Kometani, 1959; Gipps, 1981; Zheng, 2014; Yang et al., 2019). In addition, time-based indicators including TTC (time to collision), 1/TTC (the inverse TTC), THW (time headway), and some modified TTC measures are also widely used in risk evaluation (Lee, 1976; Minderhoud and Bovy, 2001; Zhao et al., 2018; Liu and Selpi, 2019; Jiao et al., 2021). Furthermore, safety margin (SM) was found to be more suitable to quantify homeostatic risk perception than TTC or THW does (Lu et al., 2012). In intersection scenarios, most of the existing studies focus on the quantification of vehicle conflict risk within the intersection area (Autey et al., 2012; Ma et al., 2018; Yang et al., 2021). At intersection approaches, the car-following behavior and traffic flow evacuation are the main objects of scholars' attention (Yu and Shi, 2014; Zhao et al., 2020b). For example, Jin et al. (2009) proposed a new car-following model to explain why the time intervals between two successive vehicles passing the stop line of the signalized intersection follow position-dependent log-normal distributions except the first one. Zhang et al. (2019) analyzed the THW distribution under different signal status and proposed a new car-following model to capture the impacts of signal status on car-following behavior. These scenario-based studies mainly focus on the interaction between vehicles, and the whole traffic environment is rarely considered globally. Later, field theory (Ni, 2013) was applied to quantify driving risks. Artificial potential field (APF) method (Kathib, 1990; Mccrone et al., 2017) regards the vehicle motion in the traffic environment as the motion in the force field, where the obstacles generate repulsive forces, the target generates gravity, and the resultant force of gravity and repulsive forces controls the direction of motion. Wang et al. put forward the driving safety field theory considering the human-vehicle–road factors, indicating the influence degree of each factor on driving safety, and describing the driving safety with physical quantities such as field strength, field force and potential energy, and the method has been developed and applied in various scenarios (Wang et al., 2016; Li et al., 2019; Zhao et al., 2020a; Zheng et al., 2021). These studies usually contribute to the trajectory and motion planning and collision avoidance control for autonomous vehicles, but cannot describe human's decision-making behaviors because different people have different levels of acceptable risk. More critically, these studies ignore the risks generated by dynamic traffic control elements such as traffic lights, and thus fail to describe approaching behaviors to signalized intersections.

In our previous study (Tan et al., 2021), traffic elements were divided into static environmental elements (including obstacles that can be crossed, such as lane lines, and impassable obstacles, such as roadblocks), moving objects (such as non-static motor vehicles, non-motor vehicles and pedestrians) and dynamic traffic control elements, and a new risk field model of the entire traffic environment was established to quantify the risk in the process of driving. In particular, the risk function corresponding to the vehicle was constructed, based on which the driver behavior model was established, which has been well verified in car-following and lane-changing scenarios. The effective fit to car-following and lane-changing behaviors also demonstrated the effectiveness of risk quantification, the basis of the behavior model. The present study will be a supplement to our previous study, specifically describes the construction process of the risk field model of dynamic traffic control elements and its constraints on vehicles. Dynamic traffic control elements here mainly refer to traffic lights set at intersections, which control the approaching behaviors of vehicles.

Therefore, our motivation is to construct a driving behavior model that can describe the risk constraints of dynamic traffic control elements (traffic lights) on vehicle movement. Taking risk perception into consideration, this study can link the change of traffic signal to drivers' decision-making and help to better understand the formation mechanism of approaching behaviors.

This paper is organized as follows. After the introduction, a driving behavior model focusing on approaching signalized intersections during yellow period is proposed in Section 2, describing the process of risk quantification and trajectory planning. Section 3 calibrates the parameters and validates the model with constant and uncertain values of human's desired risk, and the distribution of acceleration and deceleration rates when passing the stop line are obtained in the simulation. Section 4 compares the proposed model

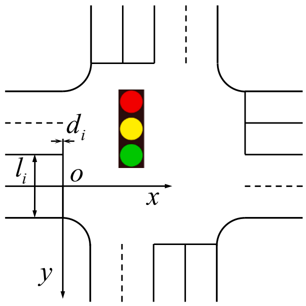

(a) Coordinate system

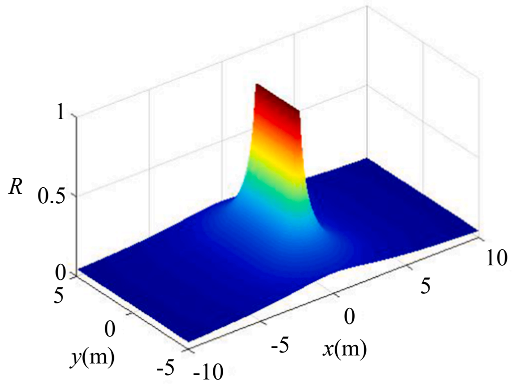

(b) All-round spatial variation of the risk

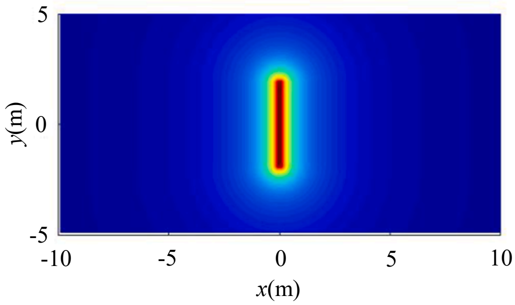

(c) All-round spatial variation of the risk (top view)

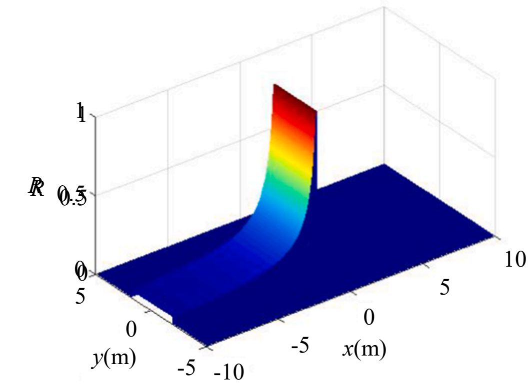

(d) Spatial variation of risk only considering the actual area of the risk

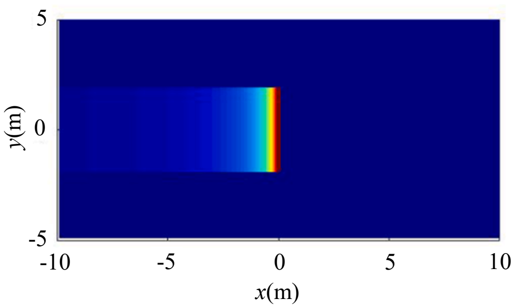

(e) Spatial variation of risk only considering the actual area of the risk (top view)

Fig. 1. Spatial variation of the risk field of traffic lights.

with existing data-driven models and discusses the effect of parameter changes on the proposed model. In Section 5, we conclude the paper with perspectives for future research.

2. Modeling

Since the traffic light controls the vehicle movement by converting different signals, it imposes different degrees of risk to vehicles when a signal is preventing them from passing the intersection. The risk can be considered at the control border, i.e., for the vehicles at intersection approaches, the risk exists at the corresponding stop lines. In this section, we describe how we construct the risk field model of traffic lights and the driving behavior model for vehicles at intersection approaches.

2.1. Risk field model of traffic lights

Different from the risk fields of static environmental elements and moving objects, the risk field of traffic lights is dynamic, whose risk values are not equal at different locations or moments. Therefore, before constructing the risk field model, we first make assumptions about the shape of the model in space and time, respectively. In space, we make two assumptions: (1) The stop line is regarded as a static obstacle. As the vehicle approaches the intersection, the risk imposed by the traffic light on the vehicle changes continuously; (2) The closer the vehicle is to the stop line, the greater the risk. In terms of time, there are four assumptions: (1) The risk imposed to the same location varies continuously over a signal period (the signal changes from green to yellow to red); (2) The maximum value of the risk is 0 during the green period and 1 during the red period; (3) When the yellow light is on, the shorter the remaining time of the yellow light, the greater the risk to a same location; (4) The risk of the yellow light increases faster as getting closer to the red light.

Based on the above assumptions, the risk field model of traffic lights is constructed. The coordinate system is established with the center of the stop line as the origin. The driving direction of the vehicle is the X-axis, and the perpendicular to the driving direction is the Y-axis, as shown in Fig. 1(a).

2.1.1. Spatial variation of risk field

For the spatial variation of traffic light risk, if a vehicle is in the position of the stop line, the risk borne by the vehicle reaches the maximum under the current signal state; while the risk value tends to be zero when the vehicle is farther away from the stop line. A parameter δ is used to show the effect of this distance relative to the stop line on the variation of risk, as shown in Eq. (1),

$$\delta_i(x,y) = \sqrt{\left[\beta_{i,x}\cdot\max(|x| - \frac{1}{2}\cdot d_i, 0)\right]^2 + \left[\beta_{i,y}\cdot\max(|y| - \frac{1}{2}\cdot l_i, 0)\right]^2} \tag{1}$$

where l_i and d_i represent the length and width of the i-th stop line, and $\beta_{i,x}$ and $\beta_{i,y}$ represent the influence degree of the relative spacing of the i-th stop line on the longitudinal and lateral risk.

For (x,y) represents the center point position of the vehicle, when both $|x|\leqslant\frac{1}{2}\cdot d_i$ and $|y|\leqslant\frac{1}{2}\cdot l_i$ are met in Eq. (1), i.e., δ_i is equal to 0, it means that the vehicle reaches the stop line, and the risk value reaches its maximum in Eq. (2). Eq. (2) means that the larger the value of δ_i, the farther away from the stop line, and the smaller the risk value. Visually, at a certain moment, the risk of signal lights presents a spatial pattern with the stop line as the center, radiating outwardly and gradually decreasing, as shown in Fig. 1(b) and 1(c).

$$R_{stopline,i}(x,y) = \frac{1}{\delta_i(x,y)+1} \tag{2}$$

The construction process of the spatial variation of the traffic light risk field model above is similar to the construction process of the lane line risk field model (Tan et al., 2021). However, since the risk of traffic lights only acts on vehicles approaching the intersection in the X-axis direction, only the spatial radiation of the stop line in the negative X-axis direction is considered in the subsequent modeling process, as shown in Fig. 1(d) and (e).

2.1.2. Time variation of risk field

As mentioned earlier, the risk of traffic lights varies not only with space, but also with time. To describe the risk as changing simultaneously over time and space, we consider to multiply the spatial variation function of risk by a coefficient to reflect the risk at different times. In terms of time, we believe that when the green light is on, the risk of traffic light is 0, indicating that vehicles can directly pass the intersection without being affected by the signal; while, when the red light turns on, the highest risk is 1, and the highest risk is located at the stop line (i.e., the value of δ_i in Eq. (2) is 0), indicating that vehicles cannot cross the stop line. In addition to the above two situations, according to the actual data, it can be found that there are also vehicles through during the yellow period. Therefore, we try to reflect the risk by the number of vehicles crossing the stop line at different times during the yellow period.

We use yellow-light running cases from high-resolution event-based data collected at six intersections along a major arterial (Trunk Highway 55) in the Twin Cities area (Liu et al., 2009; Lu et al., 2015). The data was collected by the Systematic Monitoring of Arterial Road Traffic and SIGNAL system developed at the University of Minnesota (Liu et al., 2009), and the system is capable of continuously collecting and archiving high-resolution event-based vehicle-detector actuations and signal phase change data. The cases were investigated from west to east in the direction of the particular phase, in which the green time is 110 s, yellow time is 5.5 s, and the total cycle length is 210 s. About 8 months' data (from Nov. 3rd, 2008 to Dec. 31st, 2008 and from Apr. 1st, 2009 to Sep. 23rd, 2009) were collected. Over 35,000 yellow-light running cases can be used, and the time from yellow light beginning to arriving at the stop line for each vehicle is available.

Fig. 2(a) shows the number of vehicles crossing the stop line at different time intervals during the yellow period. The decreasing number of vehicles means that fewer vehicles pass when yellow time is longer past, indicating a greater risk from the yellow light. In other words, the change in the number of vehicles is the opposite of that in risk. Hence, the reciprocals of the number of vehicles passing in each interval are taken. Since the maximum risk is 1, the reciprocal sequence is normalized and the resulting scatter points are shown in Fig. 2(b). By fitting the scatter points, it is found that the exponential function can well describe the trend of the risk change with the yellow time, where the R-squared value is 0.828. Eq. (3) is the obtained exponential function model (see Fig. 2(b)). However, the yellow light duration here is fixed, which means that this model is only applicable to the intersection where the yellow time is 5.5 s.

$$R(t) = 0.0006595e^{1.2946t} \tag{3}$$

To eliminate this limitation, the total yellow time is replaced by t_y. During the yellow period, the function of traffic light risk changing with time should meet two constraints: (1) at the moment that the green light turns off and the yellow light turns on, the risk equals to 0; (2) when the yellow light ends and the red light begins, the risk equals to 1. Therefore, on the basis of Eq. (3), the function of risk changes with time is adjusted, as shown in Eq. (4).

$$R(t) = \frac{t}{t_y}e^{\alpha(t-t_y)}, t \in [0, t_y] \tag{4}$$

Nonlinear regression analysis is performed on Eq. (4). The estimated value of parameter α is 1.719 with 95% confidence interval, [1.396, 2.042]. The R-squared value is 0.929, and the fitting effect of the model is good (see Fig. 2(b)). The established model can express the relationship between the risk and traffic light time independently of yellow duration, as shown in Eq. (5),

$$R_j(t) = \begin{cases} 0, & nT_j < t \leqslant nT_j + t_{j,g} \\ \dfrac{t-(nT_j+t_{j,g})}{t_{j,y}}e^{1.719[t-(nT_j+t_{j,g})-t_{j,y}]}, & nT_j + t_{j,g} < t \leqslant nT_j + t_{j,g} + t_{j,y} \\ 1, & nT_j + t_{j,g} + t_{j,y} < t \leqslant nT_j + t_{j,g} + t_{j,y} + t_{j,r} \end{cases} \tag{5}$$

where $t_{j,g}$, $t_{j,y}$, $t_{j,a}$, T_j are the durations of green light, yellow light, red light, and signal cycle at the j-th traffic light, and n is a natural number.

Finally, the risk field model of traffic lights can be described as Eq. (6), which is the form of multiplying the time variation function and spatial variation function,

$$R_{signal,j}(x, y, t) = R_j(t) \cdot R_{stopline,j}(x, y) \tag{6}$$

2.2. Driving behavior model of vehicles

2.2.1. Risk prediction

The preview-follower theory reflects the driver's decision on the predicted trajectory of the vehicle (Gao et al., 2000). According to the preview-follower theory, the driver will predict the state of the subject vehicle in the following time based on the current state, and expect the minimum error between the predicted and desired positions after the preview time. When there is a gap between the predicted and desired positions, the driver will consider changing the current motion state. Therefore, to find this gap, the risk field to which the vehicles affected by the traffic light will be exposed after the preview time should be predicted.

Firstly, assume that the vehicle travels at a constant speed during the preview time. The position and speed of the subject vehicle after the preview time can be calculated by Eq. (7),

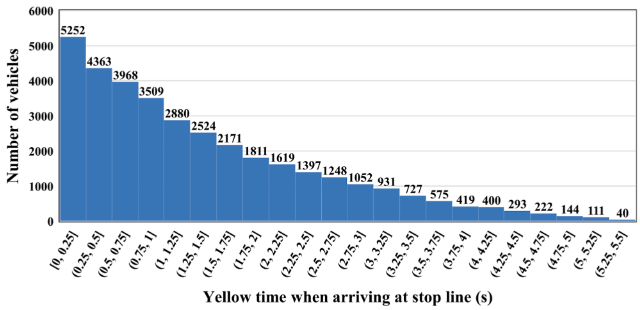

(a) Frequency histogram of the number of vehicles running yellow lights

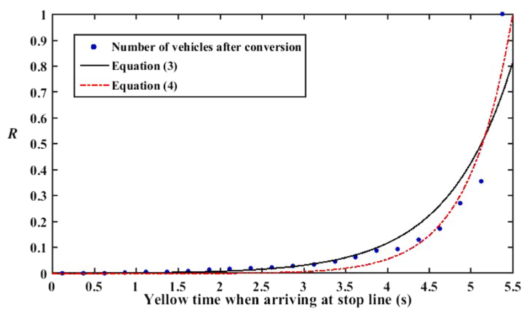

(b) Fitting curves of risk versus yellow time

Fig. 2. Fitting the relationship between risk and yellow time when arriving at stop line.

$$x_{s,p}(t+T) = x_s(t) + T \cdot \dot{x}_s(t) \tag{7}$$

where T is preview time; $x_s(t)$ and $\dot{x}_s(t)$ are the position and speed of the subject vehicle at the time t, respectively; $x_{s,p}(t+T)$ represents the predicted position of the subject vehicle at the time $t+T$.

Then, the risk generated by the traffic light after the preview time can be calculated by Eq. (8). Finally, by substituting the predicted position of the subject vehicle into the traffic light risk prediction model, the risk borne by the subject vehicle after the preview time can be obtained, which can be represented by $R_{s,p}(t+T)$, as shown in Eq. (9). The predicted risk is the basis on which the subject vehicle makes motion decisions at this time step.

$$R_{signal,p}(x, t+T) = R(t+T) \cdot R_{stopline}(x, t+T) \tag{8}$$

$$R_{s,p}(t+T) = R_{signal,p}(x_{s,p}(t+T), t+T) \tag{9}$$

2.2.2. Trajectory planning

According to the risk homeostasis theory (Wilde, 1982), a driver has a fixed desired risk and makes decisions on the basis of the difference between subjectively perceived risk and the desired risk during driving. Although the driver may over-compensate or under-compensate when he/she performs risk-compensating behaviors, the risk value always remains around the fixed value and fluctuates around it. The driver considers the risk after the preview time and make decisions based on this predicted risk. Therefore, the key point of vehicle trajectory planning is to find the desired position after the preview time according to the predicted risk.

Firstly, the risk field borne by the subject vehicle after the preview time can be predicted by Eq. (8). Then, we need to look for the desired position $x_{s,d}(t+T)$ in the predicted risk field that matches the driver's desired risk R_0. Finally, the acceleration $\ddot{x}_s(t)$ required to reach the desired position can be calculated by Eq. (10), thus completing the trajectory planning within a time step.

$$\ddot{x}_s(t) = [x_{s,d}(t+T) - x_{s,p}(t+T)]/(\frac{1}{2}T^2) \tag{10}$$

2.2.3. Trajectory planning for approaching vehicles based on risk quantification

Based on risk quantification, we conduct trajectory planning for vehicles about to enter the signalized intersection. The whole process can be divided into four steps, which are the calculation of the reachable range after the preview time, the judgment of the vehicle position, the trajectory planning for the leading vehicle and the trajectory planning for the non-leading vehicle. Fig. 3 shows

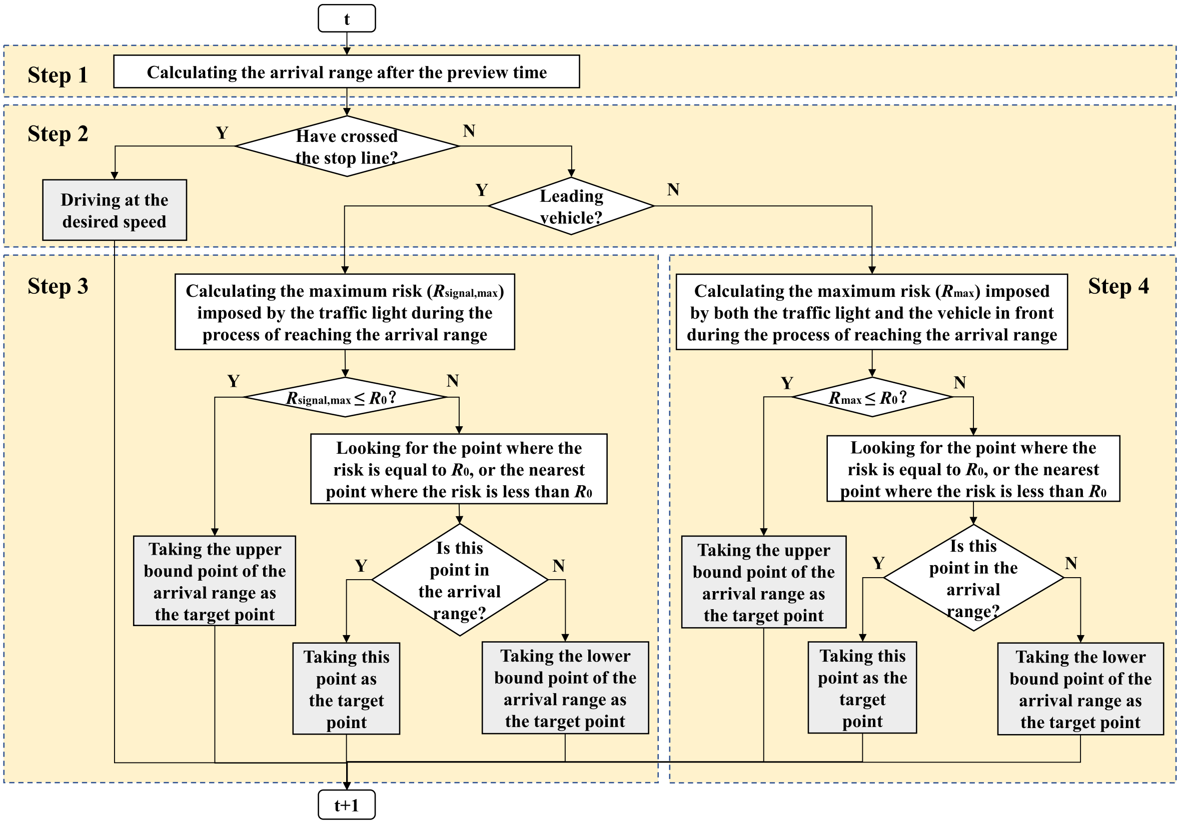

Fig. 3. Trajectory planning flow chart.

the steps for trajectory planning. The algorithm for each step is described in detail below.

Step 1. Calculation of the arrival range after the preview time.

In order to facilitate the subsequent calculation, the vehicle speed and acceleration should be constrained before planning the trajectory, as shown in Eqs. (11) and (12). Subsequently, an arrival range that the vehicle can reach after the preview time can be obtained, as shown in Fig. 4. The desired position that the vehicle looks for at each time step is within this range. The lower bound of the arrival range is the position that can be reached by the vehicle traveling at the minimum acceleration, and the upper bound of the arrival range is the position that can be reached by the vehicle traveling at the maximum acceleration. If the predicted final speed after the preview time is beyond the speed constraint, then after reaching the speed threshold, the vehicle is allowed to going a uniform speed, which is the constraint boundary of the speed. The lower bound and the upper bound of the arrival range can be calculated by Eqs. (13)-(16),

$$\dot{x}_{s,\min} \leqslant \dot{x}_s(t) \leqslant \dot{x}_{s,\max} \tag{11}$$

$$\ddot{x}_{s,\min} \leqslant \ddot{x}_s(t) \leqslant \ddot{x}_{s,\max} \tag{12}$$

$$x_{range,\min}(t+T) = x_s(t) + S_{range,\min}(t+T) \tag{13}$$

$$S_{range,\min}(t+T) = \begin{cases} \dot{x}_s(t)\cdot T + \frac{1}{2}\ddot{x}_{s,\min}T^2, & \dot{x}_s(t) + \ddot{x}_{s,\min}T \geqslant \dot{x}_{s,\min} \\ \dfrac{\dot{x}_{s,\min}^2 - \dot{x}_s^2(t)}{2\ddot{x}_{s,\min}}, & \dot{x}_s(t) + \ddot{x}_{s,\min}T < \dot{x}_{s,\min} \end{cases} \tag{14}$$

$$x_{range,\max}(t+T) = x_s(t) + S_{range,\max}(t+T) \tag{15}$$

$$S_{range,\max}(t+T) = \begin{cases} \dot{x}_s(t)\cdot T + \frac{1}{2}\ddot{x}_{s,\max}T^2, & \dot{x}_s(t) + \ddot{x}_{s,\max}T \leqslant \dot{x}_{s,\max} \\ \dfrac{\dot{x}_{s,\max}^2 - \dot{x}_s^2(t)}{2\ddot{x}_{s,\max}} + \dot{x}_{s,\max}\left[T - \dfrac{\dot{x}_{s,\max} - \dot{x}_s(t)}{\ddot{x}_{s,\max}}\right], & \dot{x}_s(t) + \ddot{x}_{s,\max}T > \dot{x}_{s,\max} \end{cases} \tag{16}$$

where $S_{\text{range,min}}(t+T)$ and $S_{\text{range,max}}(t+T)$ are the minimum and maximum displacements that the vehicle can move forward after the preview time, respectively; $x_{\text{range,min}}(t+T)$ and $x_{\text{range,max}}(t+T)$ are the lower and upper bounds of the arrival range that the vehicle can reach after the preview time, respectively.

Step 2. Determination of the vehicle position.

Vehicles in different positions are exposed to different sources of risk, and their corresponding behaviors are also different. Therefore, before trajectory planning, the second step is to determine the positions of vehicles.

Firstly, since the risk of traffic lights has no influence on the elements already located inside intersections, if the influence of other vehicles inside intersections is not considered, the vehicle that has crossed the stop line can drive at the desired speed, i.e., the upper boundary point of the arrival range can be taken as the target position. The acceleration, speed and position for the next time step can be calculated by Eqs. (17)-(19),

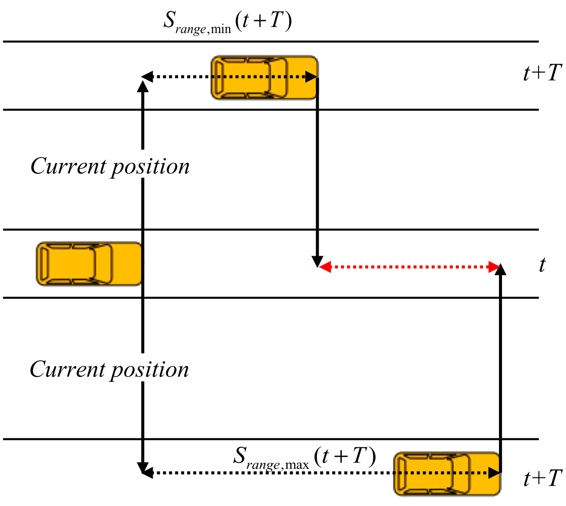

Fig. 4. Arrival range after the preview time.

$$\ddot{x}_s(t+1) = \ddot{x}_{s,\max} \tag{17}$$

$$\dot{x}_s(t+1) = \dot{x}_s(t) + \ddot{x}_{s,\max}t \tag{18}$$

$$x_s(t+1) = x_s(t) + \dot{x}_s(t)\cdot t + \frac{1}{2}\ddot{x}_s(t+1)\cdot t^2 \tag{19}$$

Additionally, the movement of a leading vehicle that has not yet crossed the stop line is directly affected by the risk of the traffic light, hence only the risk generated by the traffic light needs to be considered when predicting the risk field. While, the movement of a non-leading vehicle that has not crossed the stop line is affected by both the risk of the traffic light and the risk of the vehicle in front, so the risks generated by both should be taken into account when predicting the risk field. Step 3 and 4 will respectively describe the trajectory planning methods of these two vehicles in detail.

Step 3. Trajectory planning for leading vehicles.

First, calculate the maximum risk that the traffic light will put on the vehicle during the process of arriving at the next position after the preview time, i.e., for arriving at each point in the arrival range, a corresponding maximum risk will be generated. Then, by taking the maximum value of these maximum risks, the overall maximum risk predicted at this time step can be obtained, and the point corresponding to this risk value is the maximum risk point. By comparing this maximum risk with the desired risk, the target position can be determined. Fig. 5 shows the possible scenarios.

Based on the second assumption about the spatial variation of the risk field, it can be inferred that if the predicted upper bound of the arrival range has not yet crossed the stop line, the point with the maximum risk borne by the vehicle in the process of reaching the arrival range is at the upper bound. Further, if the maximum risk $R_{signal,\max}(t+T)$ is less than the desired risk R_0, the target trajectory position $x_{s,d}(t+T)$ is the upper bound point, $x_{range,\max}(t+T)$, as shown in Fig. 5(a).

However, if the maximum risk $R_{signal,\max}(t+T)$ is over the desired risk R_0, the point where the risk is equal to R_0 or the nearest point where the risk is less than R_0 would be sought as the preparatory target position. The next is to determine whether the preparatory point is within the arrival range. If so, this preparatory point is the final target position, as shown in Fig. 5(b); if not, the preparatory point must be in a position that does not reach the lower bound of the arrival range. However, considering the kinematic constraints, the vehicle can only take the lower bound as the target position, and the risk it bears may exceed the desired risk, as shown in Fig. 5(c).

The fourth situation is that the lower bound has crosses the stop line. In this situation, no matter which position the vehicle chooses to reach, the vehicle will bear the highest risk at the stop line, i.e., the minimum values of the predicted risks are all greater than the desired risk. The possible reason for this situation may be that when the front vehicle of a non-leading vehicle passes the stop line before the end of the yellow light, the non-leading vehicle suddenly becomes a leading vehicle. At this time, this vehicle may be about to reach the stop line and the yellow light is about to end. The driver cannot choose a point in the arrival range to avoid suffering the risk value that is higher than his/her desired risk. Due to the randomness and uncertainty of the driver's behavior, a random position

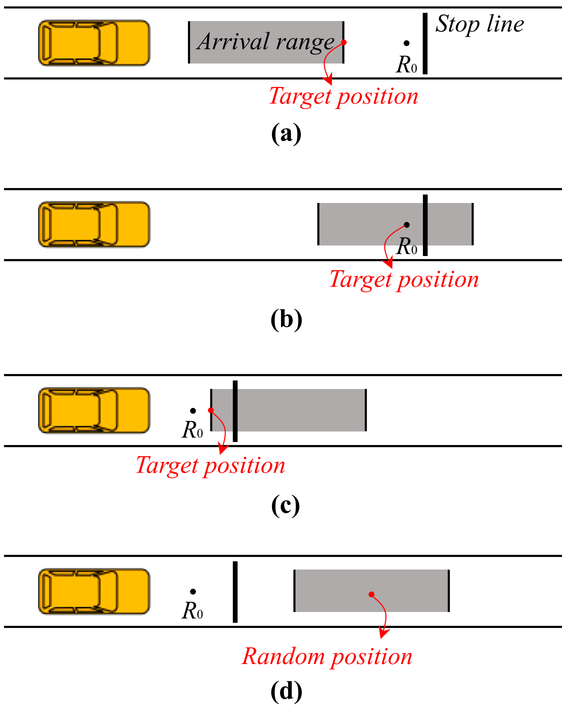

Fig. 5. Trajectory planning for the leading vehicle.

can be selected within the arrival range as the target position in this situation, as shown in Fig. 5(d).

Step 4. Trajectory planning for non-leading vehicles.

Since the movement of the following vehicle is affected by the risks of traffic lights and front vehicle, the risk field generated by the front vehicle after the preview time should be added on the basis of the previous step when predicting the risk. In our previous study, the risk of moving vehicles, varying with the relative distance and speed, has been quantified and well validated in car-following scenarios (Tan et al., 2021). The risk value in the area occupied by the vehicle as a non-crossable obstacle is the maximum value of the risk, which is consistently equal to 1. And the risk decreases continuously from 1 and tends to be 0 in all directions when the relative distance to the vehicle increases at the same speed. When the vehicles are moving, the vehicle speed also needs to be considered, and the risks increase with speeds, as shown in Fig. 6. The longitudinal risk of moving vehicles can be calculated by Eqs. (20) and (21) (Tan et al., 2021),

$$\delta_{x,k}(x,y,t)=\frac{\beta_{k,x}\cdot\max\left(|x|-\frac{1}{2}L_k,0\right)}{\alpha_{k,x}\dot{x}_{k,x}(t)+1} \tag{20}$$

$$R_{vehicle,longi,k}(x,y,t)=\frac{1}{\delta_{x,k}(x,y,t)+1} \tag{21}$$

where $\alpha_{k,x}$ and $\beta_{k,x}$ represent the influence degrees of the speed and relative distance of the k-th vehicle on the longitudinal risk, respectively; $\dot{x}_{k,x}(t)$ is the longitudinal speed of the k-th vehicle at time t; L_k is the length of the k-th vehicle.

Then the position and speed of the front vehicle after the preview time can be calculated by Eqs. (22) and (23), and its risk after the preview time can be represented by $R_F(x,t+T)$.

$$x_F(t+T)=x_F(t)+\dot{x}_F(t)\cdot T \tag{22}$$

$$\dot{x}_F(t+T)=\dot{x}_F(t) \tag{23}$$

Further, the maximum risk imposed by the front vehicle after the preview time and the position of the maximum risk can be obtained by Eqs. (24) and (25), respectively,

$$R_{F,\max}(x,t+T)=\begin{cases}R_F[x_{range,\max}(t+T),t+T], & x_{range,\max}(t+T)\leqslant x_F(t+T)-\frac{1}{2}L_{veh}\\ R_F[x_F(t+T)-\frac{1}{2}L_{veh},t+T], & x_{range,\max}(t+T)>x_F(t+T)-\frac{1}{2}L_{veh}\end{cases} \tag{24}$$

$$x_{R_{F,\max}}(t+T)=\begin{cases}x_{range,\max}(t+T), & x_{range,\max}(t+T)\leqslant x_F(t+T)-\frac{1}{2}L_{veh}\\ x_F(t+T)-\frac{1}{2}L_{veh}, & x_{range,\max}(t+T)>x_F(t+T)-\frac{1}{2}L_{veh}\end{cases} \tag{25}$$

Finally, the maximum risk that the non-leading vehicle bears after the preview time is the greater of the maximum risk of the front vehicle and the maximum risk of the traffic light, as shown in Eq. (26),

$$R_{\max}(x,t+T)=\max[R_{signal,\max}(x,t+T),R_{F,\max}(x,t+T)] \tag{26}$$

The trajectory planning method of non-leading vehicles is similar to that of leading vehicles, which are both based on the predicted risk to find the desired position after the preview time. Since the subject vehicle is always in the following state and will not exceed its leading vehicle, in fact, when the upper bound of the arrival range does not exceed the predicted position of the leading vehicle, the risk of the upper bound point is the maximum risk after the preview time. Under this premise, when the maximum risk is less than the desired risk, the target position is the upper bound point, as shown in Fig. 7(a). On the contrary, if the maximum risk is greater than the desired risk, the nearest point in the arrival range where the risk is equal to or less than the desired risk should be sought as the preparatory target point. If such a point exists in the arrival range, this point is the desired point, as shown in Fig. 7(b); if not, it must be in a position less than the lower bound, and the lower bound point can be taken as the target point, as shown in Fig. 7(c).

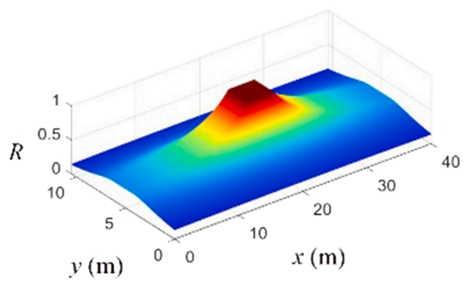

Fig. 6. Risk field of moving vehicles.

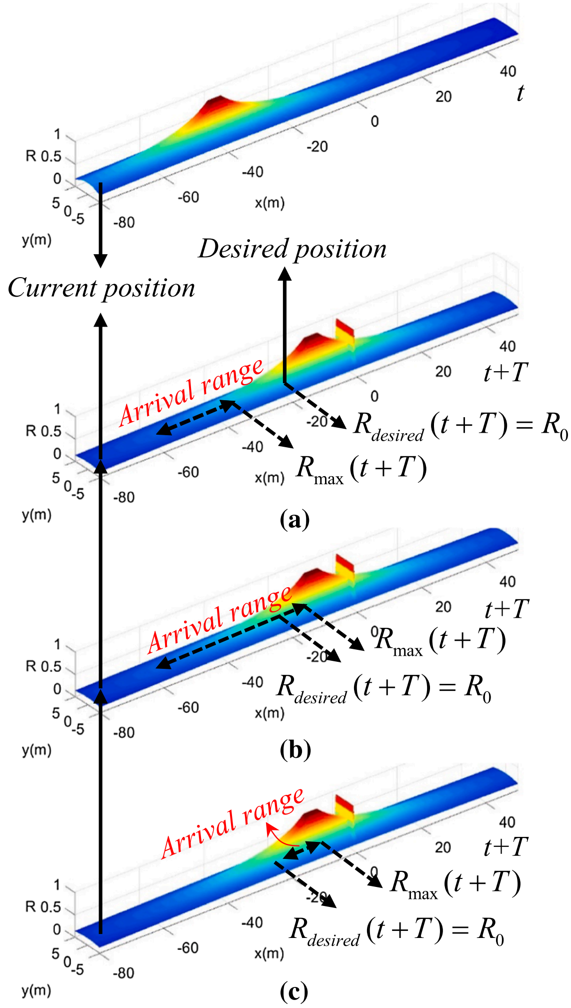

Fig. 7. Trajectory planning for the non-leading vehicle.

3. Model validation

3.1. Parameter calibration

The previous study has calibrated the parameters in the risk field model corresponding to moving vehicles (see Eqs. (20) and (21)) and the desired risk by establishing the relationship between predicted risk and THW in stable car-following processes and stopping states, where the predicted risk of the subject vehicle is considered equal to the desired risk (Tan et al., 2021). The value of α_x and β_x in Eq. (20) are respectively 0.631 and 1, and R_0 is equal to 0.345. What's more, the preview time T is taken as a constant value, 1.5 s.

For the parameter β_x in the risk field model corresponding to traffic lights shown in Eqs. (1) and (2), which is related to the spatial variation of the risk of traffic lights, the distance of 0.8 m to the edge of the stop line after stopping in red light is taken as a constraint, as the distance to the edge is observed in the NGSIM video dataset to be approximately in the range of −0.4 to 2 m (The negative value means that the vehicle has crossed the stop line when stopping). In the red state, the risk that the traffic light imposes on the vehicle can be considered equal to the desired risk R_0. Therefore, the value of β_x can be calculated by Eq. (27), and is equal to 2.373.

$$R_{signal}=\frac{1}{\beta_x\cdot 0.8+1}=R_0 \tag{27}$$

3.2. Simulation with a constant value of R_0

A number of researchers have modeled and discussed the relationship between the probability of stopping or passing and different factors related to drivers, vehicle movement states, and driving environment by analyzing the observed data. The approach speed and distance to stop line when the yellow begins are almost the two most discussed factors, which are relatively easy to collect and extract.

For instance, Yang et al. (2014) collected the data about driver behaviors at two signalized intersections located in Changchun, China during workday rush hours with video camera, where the yellow time was 3 s. A binary logistic regression model and a fuzzy decision model were established successively to describe the drivers' choices, whose percentages of correct prediction are both more than 80%. Pathivada and Perumal (2019) collected data by video capturing technique under mixed traffic conditions at five signalized intersections in Mumbai, India during non-peak hours. The average yellow time at these intersections was close to 4 s. A binary logistic regression model explained drivers' decision behaviors as a function of various explanatory variables with the prediction accuracy of 82.3%. In addition, Pawar et al. (2020) recorded 893 vehicle trajectories during yellow at three high-speed signalized intersections from 2.00 to 4.30 pm in the state of Telangana, India, where the yellow time was 3 s, and developed a binary logit model with a prediction success rate of 90.4%.

In the present study, different approach speeds and distances to the stop line when the yellow begins are put into the four models mentioned above, and the obtained results are compared with the simulation results of our driving behavior model based on risk quantification. Since the data used to develop these four models were collected under different road conditions, including different speed limits and yellow time, three different simulation conditions are set up for comparison. We write a calculation program to get the speed sequence and position sequence (starting at the beginning of the yellow light and ending at the end of the yellow light) of the vehicle approaching or crossing the stop line during the yellow period under different conditions, and they were separated by 0.1 s. These help to determine if the vehicle has crossed the stop line during the yellow period. Without considering the heterogeneity of drivers and given that R_0 is a constant value equal to 0.345, our model is simulated. The acceleration limit is set from -4 to 1.5 m/s^2 according to the study of Lu et al. (2013). The simulation results (presented by 0–1 values) of our proposed model are compared with the calculation results (calculated by the models given in the corresponding papers, and presented by percentages) of the four models in the existing studies which were modeled using real data. In the simulation results of our proposed model, if the vehicle can cross the stop line before red turns on, the result will be marked as 1; if not, mark it as 0. While the percentages represent the probability of vehicles passing the stop line during the yellow period calculated using models from existing studies. Table 1 shows the comparison results under the simulation condition with a speed limit of 60 km/h, and the yellow time is 3 s. Table 2 compares the results at speed limit 80 km/h and yellow time 3 s. The comparison results at speed limit 80 km/h and yellow time 4 s are presented in Table 3.

When the probability of passing calculated by the existing models exceeds 50%, it is considered to be consistent with the simulation

Table 1
Comparison results under the simulation condition with speed limit of 60 km/h and yellow time of 3 s.

Distance to stop line (m)	Approach speed (km/h)	Existing models: probability of passing			Proposed model: simulation result (passing = 1, non-passing = 0)	Approach speed (km/h)	Existing models: probability of passing			Proposed model: simulation result (passing = 1, non-passing = 0)
		Model 1	Model 2	Model 3			Model 1	Model 2	Model 3	
5	10	78.53%	86.60%	68.25%	1	40	94.25%	86.60%	93.24%	1
10		63.23%	86.60%	57.09%	0		88.51%	86.60%	89.51%	1
15		44.70%	36.60%	45.15%	0		78.36%	82.50%	84.07%	1
20		27.53%	36.60%	33.75%	0		62.99%	82.50%	76.56%	1
25		15.15%	17.80%	23.97%	0		44.45%	17.80%	66.90%	1
30		7.74%	17.80%	16.32%	0		27.33%	17.80%	55.57%	1
35		3.79%	17.80%	10.77%	0		15.02%	17.80%	43.63%	0
40		1.82%	17.80%	6.95%	0		7.67%	17.80%	32.38%	0
45		0.86%	17.80%	4.42%	0		3.76%	17.80%	22.86%	0
50		0.41%	17.80%	2.78%	0		1.80%	17.80%	15.50%	0
5	20	85.78%	86.60%	79.98%	1	50	96.43%	86.60%	96.24%	1
10		73.92%	86.60%	71.20%	1		92.70%	86.60%	94.07%	1
15		57.13%	45.80%	60.47%	0		85.66%	82.50%	90.75%	1
20		38.51%	45.80%	48.62%	0		73.73%	82.50%	85.85%	1
25		22.74%	17.80%	36.93%	0		56.88%	17.80%	78.97%	1
30		12.15%	17.80%	26.60%	0		38.27%	17.80%	69.91%	1
35		6.11%	17.80%	18.32%	0		22.57%	17.80%	58.98%	1
40		2.97%	17.80%	12.18%	0		12.05%	17.80%	47.08%	1
45		1.42%	17.80%	7.91%	0		6.05%	17.80%	35.51%	0
50		0.67%	17.80%	5.04%	0		2.94%	17.80%	25.41%	0
5	30	90.86%	86.60%	88.13%	1	60	97.81%	86.60%	97.94%	1
10		82.38%	86.60%	82.12%	1		95.44%	86.60%	96.72%	1
15		68.72%	82.50%	73.97%	1		90.78%	82.50%	94.80%	1
20		50.80%	82.50%	63.75%	1		82.23%	82.50%	91.85%	1
25		32.67%	17.80%	52.11%	0		68.50%	17.80%	87.46%	1
30		18.57%	17.80%	40.24%	0		50.55%	17.80%	81.19%	1
35		9.68%	17.80%	29.41%	0		32.45%	17.80%	72.76%	1
40		4.80%	17.80%	20.49%	0		18.42%	17.80%	62.31%	1
45		2.31%	17.80%	13.76%	0		9.60%	17.80%	50.57%	1
50		1.10%	17.80%	8.98%	0		4.75%	17.80%	38.76%	0

Note: model 1 is the binary logistic regression model (Yang et al., 2014), model 2 is the fuzzy decision model (Yang et al., 2014), and model 3 is the binary logit model (Pawar et al, 2020).

result of 1. It can be seen from Table 1 that the calculated results are almost identical with the simulation results, except that when the approach speed is 10 km/h and the distance to stop line is 10 m, the calculated probabilities of the three models are all over 50%; when the approach speed is 20 km/h and the distance to stop line is 15 m, the calculated probabilities of models 1 and 3 are a little more than 50%; and when the approach speed is 30 km/h and the distance to stop line is 25 m, the calculated probability of model 3 is 52.11%; while the simulation results are non-passing under these conditions. That's probably because when the vehicle is extremely close to the intersection at a low speed, the driver may engage in risky behavior (accelerating slightly to the point where the risk exceeds the desired risk) to cross the stop line before the red light turns on; while in our model, drivers are constrained by the desired risk when planning trajectories. In addition, it can be found that the calculated probabilities of models 1 and 2 partly deviate from the simulation results when the approach speed ranges from 40 to 60 km/h. The reason may be that the range of approach speed in the observed data of these two models is mostly between 10 and 30 km/h, resulting to the accuracies are not high enough in the range of 40 to 60 km/h. Therefore, compared with models 1, 2 and 3, it can be considered that our model is able to be applied to intersection approaches where the vehicle speed is almost lower than 60 km/h, for example, urban signalized intersections.

Tables 2 and 3 show the calculated probabilities of models 3 and 4 and the simulation results of our driving behavior model under the condition of high speed (the range is from 40 to 80 km/h). It can be seen that our model can generally describe the driver's decision behavior during the yellow period, where the vehicle speed can reach 80 km/h, for instance, the roads connecting the urban area and the suburban area.

However, there are differences in human's actual driving behaviors, and even at the same approach speed and distance to stop line, conservative and radical drivers tend to make different decisions due to their different desired risks or acceptable risks. Therefore, it is necessary to further study the simulation effects of our driving behavior model with uncertain values of R_0, i.e., to express the simulation results by probabilities of passing rather than 0–1 values.

3.3. Simulation with uncertain values of R_0

In a same driving scenario, different drivers tend to have different desired driving risks, thereby making different decisions and operations. We assume that the desired risks of all drivers fluctuate around 0.345; meanwhile, according to our trajectory planning model, when drivers arrive at the stop line, the risks borne by them are close to their respective desired risks. Therefore, we simply assume that the risk borne by drivers when arriving at the stop line is 0.345. According to the risk homeostasis theory, drivers are looking for the points with their desired risks and making corresponding acceleration or deceleration operations to be close to those target points at every moment when approaching the intersection. In other words, after crossing the stop line, the event data with acceleration of 0 can be regarded as the cases with drivers' actual desired risks equal to 0.345; if the drivers accelerate, it means that their actual desired risks are greater than the assumed value of 0.345; otherwise, the desired risks are less than 0.345. We use the acceleration distribution after the vehicles pass the stop line to obtain the distribution of drivers' desired risks. The acceleration data was extracted from the yellow-light running cases collected at six intersections along Trunk Highway 55 in the Twin Cities area as well, which can be calculated from the speed and time differences between two points. One of the two points is at the stop line, where the stop-bar detector was located; the other is at the downstream link entrance, where the entrance detector was installed. Hence the speed

Table 2
Comparison results under the simulation condition with speed limit of 80 km/h and yellow time of 3 s.

Distance to stop line (m)	Approach speed (km/h)	Existing model: probability of passing in model 3	Proposed model: simulation result (passing = 1, non-passing = 0)	Approach speed (km/h)	Existing model: probability of passing in model 3	Proposed model: simulation result (passing = 1, non-passing = 0)	Approach speed (km/h)	Existing model: probability of passing in model 3	Proposed model: simulation result (passing = 1, non-passing = 0)
10	40	89.51%	1	50	94.07%	1	60	96.72%	1
20		76.56%	1		85.85%	1		91.85%	1
30		55.57%	1		69.91%	1		81.19%	1
40		32.38%	0		47.08%	1		62.31%	1
50		15.50%	0		25.41%	0		38.76%	1
60		6.56%	0		11.54%	0		19.51%	0
70		2.62%	0		4.76%	0		8.49%	0

Distance to stop line (m)	Approach speed (km/h)	Existing model: probability of passing in model 3	Proposed model: simulation result (passing=1, non-passing=0)	Approach speed (km/h)	Existing model: probability of passing in model 3	Proposed model: simulation result (passing=1, non-passing=0)
10	70	98.21%	1	80	99.03%	1
20		95.44%	1		97.50%	1
30		88.92%	1		93.71%	1
40		75.44%	1		85.09%	1
50		54.04%	1		68.60%	1
60		31.05%	0		45.55%	1
70		14.71%	0		24.26%	0

Table 3
Comparison results under the simulation condition with speed limit of 80 km/h and yellow time of 4 s.

Distance to stop line (m)	Approach speed (km/h)	Existing model: probability of passing in model 4	Proposed model: simulation result (passing = 1, non-passing = 0)	Approach speed (km/h)	Existing model: probability of passing in model 4	Proposed model: simulation result (passing = 1, non-passing = 0)	Approach speed (km/h)	Existing model: probability of passing in model 4	Proposed model: simulation result (passing = 1, non-passing = 0)
10	40	89.79%	1	50	94.90%	1	60	97.53%	1
20		83.85%	1		91.48%	1		95.79%	1
30		74.54%	1		86.10%	1		92.92%	1
40		62.81%	1		78.14%	1		88.33%	1
50		49.35%	0		67.35%	1		81.37%	1
60		35.99%	0		54.34%	1		71.59%	1
70		24.49%	0		40.71%	0		59.24%	1
80		15.76%	0		28.37%	0		45.61%	0
90		9.74%	0		18.60%	0		32.61%	0
100		5.86%	0		11.65%	0		21.82%	0

Distance to stop line (m)	Approach speed (km/h)	Existing model: probability of passing in model 4	Proposed model: simulation result (passing = 1, non-passing = 0)	Approach speed (km/h)	Existing model: probability of passing in model 4	Proposed model: simulation result (passing = 1, non-passing = 0)
10	70	98.82%	1	80	99.44%	1
20		97.96%	1		99.03%	1
30		96.52%	1		98.33%	1
40		94.13%	1		97.14%	1
50		90.24%	1		95.14%	1
60		84.21%	1		91.86%	1
70		75.47%	1		86.69%	1
80		63.97%	1		78.98%	1
90		50.60%	0		68.44%	0
100		37.14%	0		55.58%	0

Note: model 4 is the binary logistic regression model (Pathivada and Perumal, 2019).

and time when arriving at the stop line and entrance can be obtained to calculated the acceleration. In addition, the distance between stop-bar and entrance detectors is only 105 ft, so it is reasonable to assume that most of drivers do not change their acceleration rates within such a short distance (Lu et al., 2015). Totally 35,691 cases were collected, and the mean value of accelerations for all cases is 0.3697 m/s^2 with a standard deviation of 1.6023 m/s^2 (see Fig. 8). Since the risk is defined between 0 and 1, we perform min–max normalization on the acceleration data to make the result fall into the interval [0,1]. The transformation function is as follows:

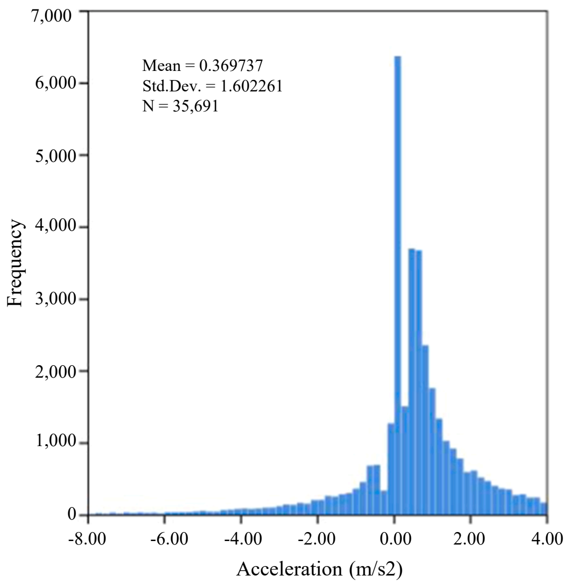

Fig. 8. Distribution of acceleration.

$$a^{*} = \frac{a - min}{max - min} \tag{28}$$

where max is the maximum value and min is the minimum value of the acceleration data.

Subsequently, a coefficient is multiplied over the normalized acceleration values, which are converted to the desired risk values (see Fig. 9). It is obvious that the distribution of desired risks is skewed. We use the median which can represent the centralization trend of skewness distribution as the desired risk value, and under different simulation conditions, it is found that the simulation results are almost consistent with the results obtained when the average value is used as the desired risk value. Therefore, the negatively skewed distribution here can be regarded as approximately normally distributed, with a mean value of 0.3403 and a standard deviation of 0.0658, which is considered to have only a slight effect on the subsequent simulation results.

Based on the distribution of desired risks, the Monte Carlo method is used, which is a numerical calculation method used for statistical simulation. The core of the method is to approximate the object of the actual problem studied by simulating a large number of sample sets or random processes. In the present study, the Monte Carlo method is implemented by writing a calculation program. According to the distribution parameters of desired risks, we randomly simulated 300 cases of drivers with different desired risks approaching the intersection at each approach speed and distance to stop line, and obtained the probabilities of vehicles passing the stop line during the yellow period. Fig. 10 shows the comparison results under the simulation conditions with different speed limits and yellow times. With a 50% probability of passing as the comparison boundary, color blocks indicate that the simulation results are consistent with the calculated results of models 1, 2, 3 or 4, while slash lines indicate that the results are inconsistent.

According to the findings discussed in Section 3.2, the calculated results of models 1 and 2 within the approach speed range of 40–60 km/h under the condition with speed limit of 60 km/h and yellow time of 3 s are ignored. Therefore, Fig. 10(a) and 10(b) show the proportions of consistency between our proposed model and models 1 and 2 within the approach speed range of 10–30 km/h, which are at least 88% and 94%, respectively; the consistency rates of more than 88% between our proposed model and model 3 are shown in Fig. 10(c), and the rate even reaches 100% at the approach speed of 60 km/h (within the range of 0–50 m, and the simulation interval is 1 m). As shown in Fig. 10(d) and 10(e), under the simulation conditions with speed limit of 80 km/h and yellow times of 3 s and 4 s, our proposed model shows a high consistency rate with models 3 and 4, respectively. It is worth mentioning that the estimated travel time (equal to distance to stop line divided by approach speed) in the actual event data is found to generally do not exceed the corresponding yellow time, so the inconsistencies in the results above 90 m where the estimated travel time is longer than 4 s in Fig. 10 (e) can be ignored. To be concluded, our mechanism-based driving behavior model shows better general applicability than the other compared models under different simulation conditions.

However, given that at some combinations of approach speed and distance to stop line, drivers' decisions may be obvious, and there is a clear consistency between models, we eliminate these combinations and further evaluate the consistency between models. We find out the combinations that (1) the driver cannot pass the stop line during the yellow period even when driving at maximum acceleration, and (2) the driver can pass the stop line even when driving at maximum deceleration, which are represented by several polylines in Fig. 10. In each subgraph, the cases above the top polylines correspond to (1), and those below the bottom polylines correspond to (2). In these cases, the results are almost consistent regardless of which model is used. By observing the consistency between each pair of polylines, it is found that (1) in Fig. 10(a) and (b), when the approach speed is 10, 20 and 30 km/h, the proportions of consistency between our model and model 1 are 60%, 80% and 86%, and those between our model and model 2 are 80%, 93% and 86%, respectively; when the approach speed is 10, 20, 30, 40, 50 and 60 km/h, the proportions of consistency between our

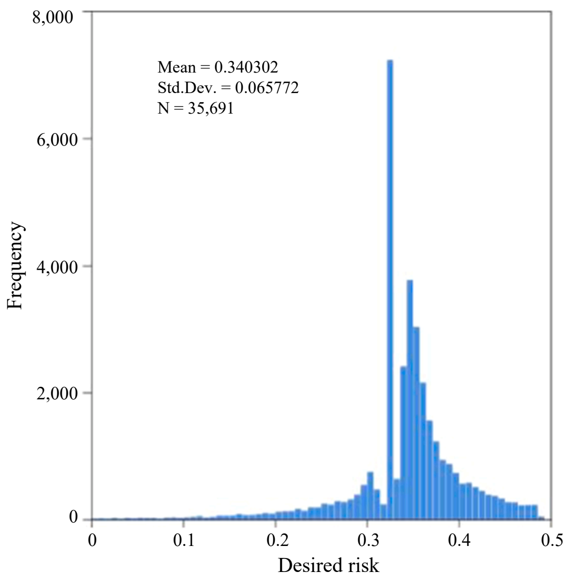

Fig. 9. Distribution of desired risk.

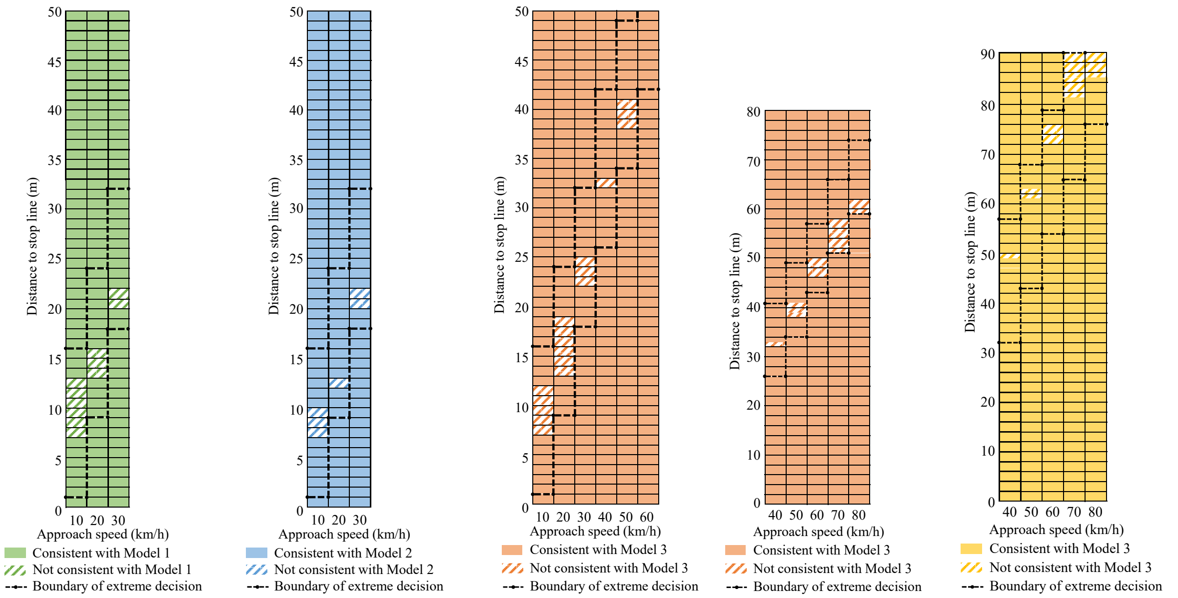

(a) Speed limit is 60 km/h and yellow time is 3 s (Compared with model 1) **(b)** Speed limit is 60 km/h and yellow time is 3 s (Compared with model 2) **(c)** Speed limit is 60 km/h and yellow time is 3 s (Compared with model 3) **(d)** Speed limit is 80 km/h and yellow time is 3 s (Compared with model 3) **(e)** Speed limit is 80 km/h and yellow time is 4 s (Compared with model 4)

Fig. 10. Comparison results of passing probabilities.

model and model 3 are 67%, 60%, 79%, 94%, 80% and 100%, respectively; (2) in Fig. 10(d), when the approach speed is 40, 50, 60, 70 and 80 km/h, the proportions of consistency between our model and model 3 are 93%, 80%, 71%, 53% and 86%, respectively; (3) in Fig. 10(e), when the approach speed are 40, 50, 60 and 70 km/h, the proportions of consistency between our model and model 4 are 96%, 92%, 84% and 60%, respectively. As mentioned above, the inconsistency between our model and model 4 within the distance to stop line above 90 m in Fig. 10(e) can be ignored. The above results show that the consistency between the simulation results of our model and the calculation results of models 1, 2, 3 and 4 is almost satisfactory.

Accordingly, different from the compared models (models 1, 2, 3 and 4 in this paper and other models not mentioned), our model is

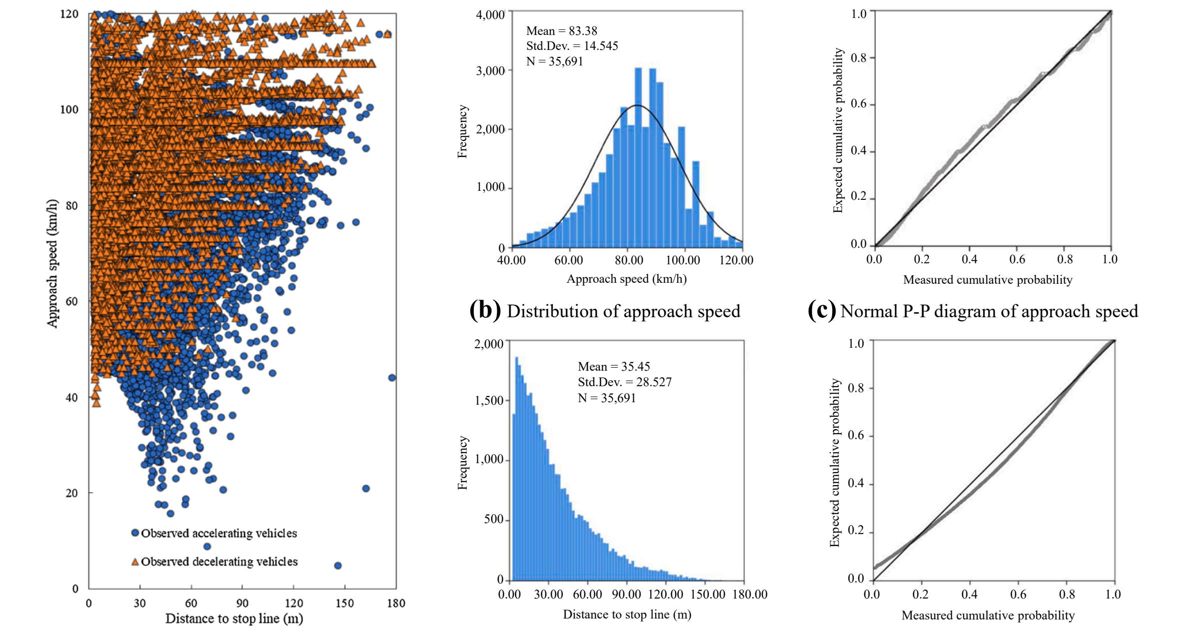

(a) Scatter of distance to stop line versus approach speed **(b)** Distribution of approach speed **(c)** Normal P-P diagram of approach speed **(d)** Distribution of distance to stop line **(e)** Semi-normal P-P diagram of distance to stop line

Fig. 11. Distribution of approach speed and distance to stop line.

proposed based on human cognitive and behavior mechanism rather than data-driven, and is able to represent drivers' risk perception and decision-making processes under different conditions, not limited by road conditions for data collection. The results can also justify the use of risk homeostasis theory to understand and model driver behaviors.

3.4. Acceleration and deceleration rates

Vehicles' acceleration rates at the time when crossing the stop line during yellow are also investigated, which are strongly related to drivers' decision of yellow-light running (Amer et al., 2011; Sharma et al., 2011; Lu et al.,2015). 23,105 accelerating cases are found among the vehicles running the yellow light, accounting for 64.74% of all cases we collected. To restore the simulation conditions similar to the actual situation as much as possible, the distribution characteristics of approach speed and distance to stop line in the collected data are explored (see Fig. 11). The mean value of approach speeds for all cases is 83.38 km/h with a standard deviation of 14.545 km/h, and the P-P diagram can prove that the approach speeds obey a normal distribution (see Fig. 11(b) and (c)). Additionally, the frequency distribution of distance to stop line is monotonically decreasing with a mean value of 35.45 m and a standard deviation of 28.527 m, and is able to pass the semi-normal distribution test (see Fig. 11(d) and (e)). Consequently, the speeds and distances to stop line of the approaching vehicles at the beginning of the yellow light are randomly selected according to their respective distributions in the simulation. Since the observed maximum acceleration rate is nearly 4 m/s^2 and the maximum deceleration rate is about 8 m/s^2, the acceleration range between -8 to 4 m/s^2 is set.

Fig. 12 shows the cumulative distribution function (CDF) curves of observed and simulated acceleration and deceleration rates at stop line. Under a constant value of R_0 equal to 0.345, 8,000 cases are simulated, and 7,905 cases of yellow-light running were obtained, accounting for 98.81%. Among them, 4,672 cases accelerate through the stop line, accounting for 59.10%. Analogously, due to the uncertain values of R_0, 20,000 simulations are performed, including 19,776 cases pass during yellow period, accounting for 98.88%, and 58.70% of them are found to be accelerating vehicles. Therefore, the yellow-light-running drivers are generally accelerating when they pass through intersections, in line with the actual collected data and the findings of previous studies (Lu et al., 2015). Compared with the CDF curves of observed vehicles, the CDF curves of simulated vehicles have a smoother slope in the acceleration range of 0.5 to 1 m/s^2 and a steeper slope in the deceleration range of 1 to 2 m/s^2. From the perspective of behavioral mechanism, accelerating drivers tend to speed up as much as possible to achieve the desired level of safety, i.e., to pass the intersection earlier, but when actually close to the intersection, they may be affected by other interference factors, such as surrounding traffic participants (Gates et al., 2007), and thus choose a lower acceleration rate. At lower percentiles (i.e., 60th percentile and lower), the deceleration rates simulated are very similar to those observed; while at higher percentiles, the deceleration rates simulated are increasingly lower than those observed. In the observed cases, more drivers are likely to use higher deceleration rates to decrease the speeds entering the intersection, improving the safety in situations where there may be vehicle interaction inside the intersection. Additionally, the distributions of acceleration and deceleration rates under the fixed R_0 and random R_0 do not show a significant difference. Despite the potential errors between the simulated and observed cases caused by some practical factors, the proposed model should be further improved in terms of parameter calibration and consideration of more factors to reduce the errors from the observed cases.

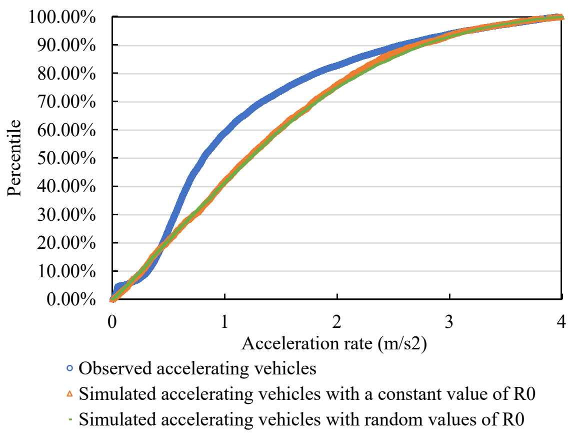

(a) Acceleration rates

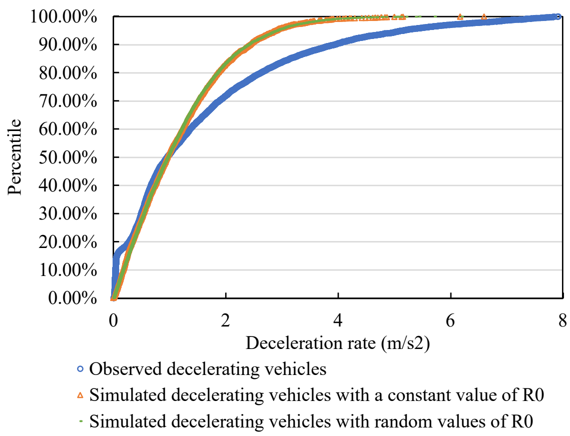

(b) Deceleration rates

Fig. 12. CDF of acceleration and deceleration rates at stop line.

4. Discussion

4.1. Theory-driven modeling vs. data-driven modeling

Driving behavior models can be divided into theory-driven models and data-driven models. Admittedly, the improvement of data collection capabilities has promoted the development of data-driven models, e.g., fuzzy logic model, regression model, and models based on non-parametric method (e.g., machine learning, (Rahman et al., 2021), etc.), which focus on the effect of fitting real traffic behaviors and enable modelers to obtain high prediction accuracy. However, the datasets used by different data-driven models are usually collected from different traffic environments, as well as the evaluation indicators and methods of the models cannot be compared systematically. That means, the data-driven models sometimes cannot give the same results about the probability of passing or stopping during the yellow period under the same traffic conditions (can be seen in Table 1), nor can they be evaluated as being better or worse. In addition, the area of interest of data-driven models mainly lies in the improvement of prediction accuracy, and they can barely explain real traffic phenomena. Taking models 1, 2, 3 and 4 mentioned in Section 3 as the examples (see Table 4), the dataset of models 1 and 2 was collected at urban intersections during workday rush hours, and those of models 3 and 4 were respectively collected at high-speed intersections and under mixed traffic conditions during non-peak hours. The prediction accuracies of models 1, 2 and 4 were calculated to prove whether they could perform well in reflecting driver behaviors; while in model 3, the sensitivity and specificity were used as statistical measures for evaluating the performance of a binary classification test. Hence, at the mercy of the differences in traffic flow, road speed limit and participant types in data collection environments, these data-driven models are highly targeted and have limitations when applied to other environments.

Compared with data-driven models, theory-driven models have definite structures and clear physical meanings. Theory-driven models have been widely used, focusing on making assumptions about driver response. Most traffic accidents are attributable to driver behaviors in response to the traffic environment, because responses to the environment vary with drivers' abilities of risk perception. Before making an operation, a driver will experience the process of risk perception, followed by comparing the perceived risk with the desired risk and making a decision. Based on the risk homeostasis theory and preview-follower theory, we apply the field theory to the driving behavior model, regarding the dynamic traffic control elements as the risk source, and the driving behavior as the compensation in response to the risk, thereby describing the vehicle movement during the yellow period from the perspective of human behavioral mechanism. This modeling method can help to understand the process of making decisions and behaviors in essence, and is not limited by the environment in which data is collected. In our model, we consider the yellow light duration, approach speed and distance to stop line of the vehicle at the onset of yellow, and these parameters can be adjusted to meet different simulation needs. Furthermore, our model can take into account the differences in the desired risk levels of different drivers, which is advanced than most traditional driving behavior models.

4.2. Considering the reaction time of drivers or autonomous vehicles

In many urban signalized intersections in some Asian countries including China, infrastructures like countdown timers are widely installed to display the remaining time of the current signal phase (Long et al., 2013; Fu et al., 2016). A green phase countdown timer is able to warn that the right of way will soon be terminated and remind drivers to timely make decisions when the yellow light is about to turn on, and sometimes a green flasher can do the same. If the countdown timer or green flasher is absent, the driver will usually have to take a reaction time before making a decision. Here the reaction time is defined as the interval between the time when the yellow turns on and the time when the driver makes a decision. The vehicle maintains the original approach speed during the reaction time and then reaches the desired position by the acceleration calculated as follows.

$$\ddot{x}_s(t+t_r) = [x_{s,d}(t+t_r+T) - x_{s,p}(t+t_r+T)]/(\frac{1}{2}T^2) \tag{29}$$

where t_r is the reaction time, which is only considered during the yellow period; $\ddot{x}_s(t+t_r)$ is the acceleration at $t+t_r$; $x_{s,d}(t+t_r+T)$ and $x_{s,p}(t+t_r+T)$ are the desired and predicted positions at $t+t_r$, respectively.

When constructing the driving behavior model, the reaction time was not considered separately, for the reason that the reaction process is included in the preview process, and these two processes are mostly synchronized. However, to investigate the effect of reaction time, the reaction time and the preview time need to be considered separately (Tan et al., 2021). According to the past studies on driver reaction times, a total reaction time of 2 s is reasonable (Setti et al., 2007; Fu et al., 2016). Therefore, a reaction time of 0.5 s is set in the simulation, and the probabilities of passing obtained are compared with that without considering the reaction time. Figs. 13-15 show that at the same approach speed and distance to stop line, the probability of passing during the yellow period is significantly reduced when there is no countdown timer compared with the case with a countdown timer. This finding is consistent with that of Yang, et al. (2014) who built a fuzzy decision tree model to predict the probability of stopping at the intersection whether a countdown timer is installed. This result may be explained by the fact that the existence of reaction time means the lag of decision time. If a driver who tends to run the yellow light does not take an excessive acceleration, he/she may not be able to pass during the yellow period, leading to a more dangerous red-light running behavior. Besides, when a driver starts to make a decision, he/she may slow down due to the greater previewed risk, and as a result, he/she is likely to stop during the red or even yellow phase. These are all potential reasons for the lower probabilities of passing.

The development of intelligent and connected vehicles requires human driving strategies to be embedded into intelligent driving systems. Vehicles with networking capabilities can receive traffic control information in advance, and there is no need to spend extra

Table 4
Differences between models 1, 2, 3 and 4.

No.	Collection time	Collection location	Evaluation indicator	Type of model	Figure
Model 1	workday rush hours	urban intersections	prediction accuracy	binary logistic regression model	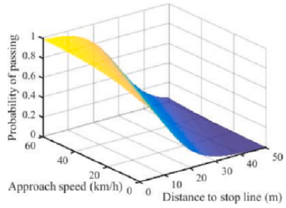
Model 2	workday rush hours	urban intersections	prediction accuracy	fuzzy decision model	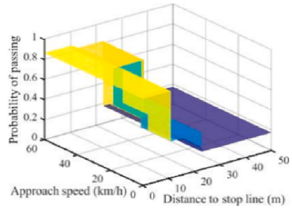
Model 3	the daytime from 2.00 to 4.30 pm	high-speed intersections	sensitivity and specificity	binary logit model	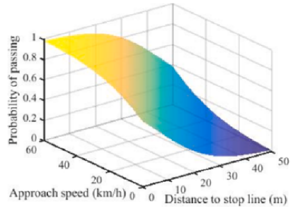
Model 4	non-peak hours	mixed traffic conditions	prediction accuracy	binary logistic regression model	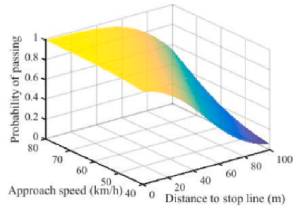

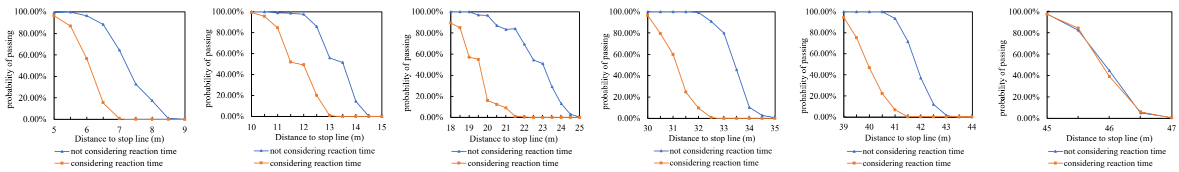

(a) Approach speed: 10 km/h **(b)** Approach speed: 20 km/h **(c)** Approach speed: 30 km/h **(d)** Approach speed: 40 km/h **(e)** Approach speed: 50 km/h **(f)** Approach speed: 60 km/h

Fig. 13. Comparison results of passing probabilities considering reaction time or not under speed limit 60 km/h and yellow time 3 s.

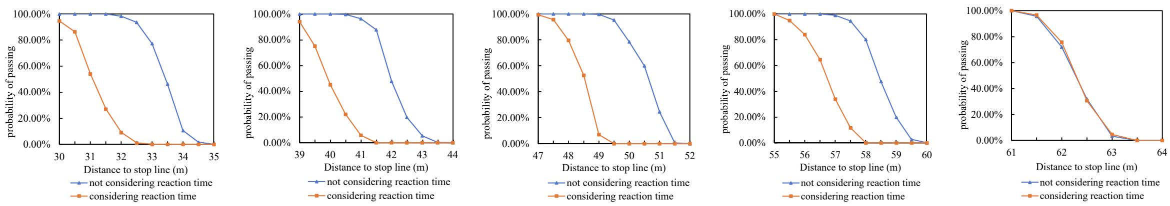

(a) Approach speed: 40 km/h **(b)** Approach speed: 50 km/h **(c)** Approach speed: 60 km/h **(d)** Approach speed: 70 km/h **(e)** Approach speed: 80 km/h

Fig. 14. Comparison results of passing probabilities considering reaction time or not under speed limit 80 km/h and yellow time 3 s.

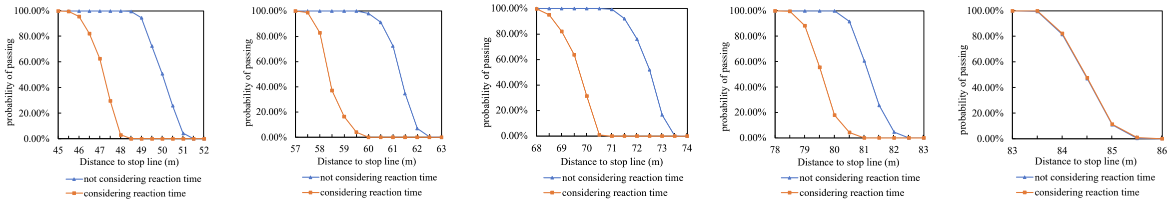

(a) Approach speed: 40 km/h **(b)** Approach speed: 50 km/h **(c)** Approach speed: 60 km/h **(d)** Approach speed: 70 km/h **(e)** Approach speed: 80 km/h

Fig. 15. Comparison results of passing probabilities considering reaction time or not under speed limit 80 km/h and yellow time 4 s.

time for human drivers to respond to sudden changes in signal lights, but the communication delay should be considered. Furthermore, controllers also need reaction time to manipulate vehicles, which is related to the performance of intelligent driving systems. Therefore, different vehicles require different reaction times to make decisions when facing the onset of yellow. The proposed model can not only describe human behaviors, but can also be applied to human-like control of intelligent vehicles. By adjusting the reaction time, and setting the corresponding speed limit value and acceleration threshold value according to the road conditions and the needs of occupants, the purpose of personalized human-like control is able to be achieved.

5. Conclusions

In this paper, we propose a risk field model to quantify the risk constraints of dynamic traffic control elements on vehicle movement, especially the coupling of time and space characteristics of the risk generated by traffic lights. Since the yellow duration in our risk field model is a variable that can be adjusted according to road conditions, the model can be applied to signalized intersections with different yellow durations, whose universality is improved. Based on the risk homeostasis theory and preview-follower theory, a trajectory planning model is subsequently developed to plan the motion and trajectories approaching signalized intersections. Drivers' dilemma during yellow period is described from the perspective of behavioral mechanism by establishing the driving behavior model framework. Drivers' desired risk is taken into account, and the different values of desired risk that adapt to individual characteristics are set in the simulation. By configuring different parameter combinations (i.e., approach speed and distance to stop line when yellow turns on and yellow time), the probability of passing the stop line obtained by the simulation is almost consistent with that calculated by the existing models, and the distribution of acceleration and deceleration rates when passing obtained by the random simulation of the Monte Carlo method is roughly consistent with that from the collected real-world driving cases, which prove the accuracy of the proposed model. We provide significant insights into the differences between different modeling frameworks, presenting considerations regarding the superiority of modeling based on human behavioral mechanisms compared to data-driven modeling. The simulation and discussion considering the reaction time show the potential of the proposed model to be applied to the motion control of intelligent vehicles.

The urban traffic environment is complex, and different types of traffic elements together constitute a risky environment. These risk elements are related to human interests and impose ubiquitous constraints on vehicle movement. Therefore, to deal with more complex driving tasks, comprehensive modeling of traffic risks is a potential solution. Our work in this paper contributes to develop a model describing driving behavior approaching signalized intersections during yellow period, with a focus on quantifying the risk imposed by dynamic traffic control elements. In addition to the risk elements mentioned in this paper, we have modeled the risks of static environmental elements and moving objects in previous study (Tan et al., 2021). These studies have a unified definition of risk and can complement each other to form a complete risk field model. By combining risk homeostasis theory and preview-follower theory, they can well describe the behavioral mechanism of drivers and provide unified rules for vehicle movement, reflecting the possibility of further development of driving behavior models.

Some limitations and future work should be concerned. (1) When modeling the risk field of traffic lights, the influence of some other non-quantifiable factors on the risk was ignored, such as intersection characteristics (number of arms, monitoring facilities, etc.), which are difficult to assess and should be considered further. (2) More microscopic trajectory data should be collected, and model parameters should be calibrated more precisely, as errors exist yet between drivers' choices of acceleration when passing the stop line between the simulated and observed cases. (3) Although the trajectory planning model includes both leading and non-leading vehicles, only the former approaching intersections during yellow period are simulated, and influences of car following and other interference from other vehicles need further exploration. (4) In the simulation verification of the model, the distribution of acceleration after crossing the stop line is transformed into the distribution of desired risk. The rationality of this approach needs to be expanded. Exploring the distribution of desired risk requires a large number of driving behavior data of different drivers, which is a difficult and worthwhile task. (5) By adjusting model parameters, to study the impacts of mixed queue composed of intelligent vehicles of different levels on traffic efficiency at intersections is of great value.

CRediT authorship contribution statement

Jun Hua: Formal analysis, Methodology, Software, Validation, Visualization, Writing – original draft. **Guangquan Lu:** Conceptualization, Funding acquisition, Project administration, Resources, Supervision, Writing – review & editing. **Henry X. Liu:** Data curation, Resources.

Declaration of Competing Interest

The authors declare that they have no known competing financial interests or personal relationships that could have appeared to influence the work reported in this paper.

Acknowledgements

This work was supported by the National Key R&D Program of China under Grant 2018YFB1600500 and the National Natural Science Foundation of China under Grant 52131204.

References

Amer, A., Rakha, H., El-Shawarby, I., 2011. Agent-based behavioral modeling framework of driver behavior at the onset of yellow indication at signalized intersections. In: 2011 14th International IEEE Conference on Intelligent Transportation Systems (ITSC). IEEE, pp. 1809-1814.
Autey, J., Sayed, T., Zaki, M.H., 2012. Safety evaluation of right-turn smart channels using automated traffic conflict analysis. Accid. Anal. Prev. 45, 120–130.
Caird, J.K., Chisholm, S.L., Edwards, C.J., Creaser, J.I., 2007. The effect of yellow light onset time on older and younger drivers' perception response time (PRT) and intersection behavior. Transp. Res. Part F 10 (5), 383–396.
Chang, M.S., Messer, C.J., Santiago, A.J., 1985. Timing traffic signal change intervals based on driver behavior. Transp. Res. Rec. 1027, 20–30.
Chen, C., Chen, Y., Ma, J., Zhang, G., Walton, C.M., 2018. Driver behavior formulation in intersection dilemma zones with phone use distraction via a logit-Bayesian network hybrid approach. J. Intell. Transport. Syst. 22 (4), 311–324.
Choudhary, P., Velaga, N.R., 2019. Driver behaviour at the onset of yellow signal: a comparative study of distraction caused by use of a phone and a music player. Transp. Res. Part F 62, 135–148.
Dong, S., Zhou, J., 2020. A comparative study on drivers' stop/go behavior at signalized intersections based on decision tree classification model. J. Adv. Transport. 2020 (2), 1–13.
El-Shawarby, I., Amer, A., Rakha, H., 2008. Driver stopping behavior on high-speed signalized intersection approaches. Transp. Res. Rec. 2056 (1), 60–69.
Fu, C., Zhang, Y., Bie, Y., Hu, L., 2016. Comparative analysis of driver's brake perception-reaction time at signalized intersections with and without countdown timer using parametric duration models. Accid. Anal. Prev. 95 (pt.B), 448–460.
Gao, Z.H., Guan, X., Guo, K.H., 2000. Driver directional control model and the application in the research of intelligent vehicle. China J. Highway Transport 13 (3), 106–109.
Gates, T.J., Noyce, D.A., Laracuente, L., Nordheim, E.V., 2007. Analysis of dilemma zone driver behavior at signalized intersections. Transp. Res. Rec. 2030, 29–39.
Gates, T.J., Noyce, D.A., 2010. Dilemma zone driver behavior as a function of vehicle type, time of day, and platooning. Transp. Res. Rec. 2149 (1), 84–93.
Gazis, D., Herman, R., Maradudin, A., 1960. The problem of the amber signal light in traffic flow. Oper. Res. 8 (1), 112–132.
Gipps, P.G., 1981. A behavioural car-following model for computer simulation. Transp. Res. Part B 15 (2), 105–111.
Gugerty, L., McIntyre, S.E., Link, D., Zimmerman, K., Tolani, D., Huang, P., Pokorny, R.A., 2014. Effects of intelligent advanced warnings on drivers negotiating the dilemma zone. Hum. Factors 56 (6), 1021–1035.
Hurwitz, D.S., Wang, H., Knodler, M.A., Ni, D., Moore, D., 2012. Fuzzy sets to describe driver behavior in the dilemma zone of high-speed signalized intersections. Transp. Res. Part F 15 (2), 132–143.
Jiao, S., Zhang, S., Zhou, B., Zhang, L., Xue, L., 2021. Dynamic performance and safety analysis of car-following models considering collision sensitivity. Physica A 564, 125504. https://doi.org/10.1016/j.physa:2020.125504.
Jin, X., Zhang, Y.i., Wang, F.a., Li, L.i., Yao, D., Su, Y., Wei, Z., 2009. Departure headways at signalized intersections: a log-normal distribution model approach. Transp. Res. Part C 17 (3), 318–327.
Kathib, O., 1990. Real-time obstacle avoidance for manipulators and mobile robots. In: Cox, I.J., Wilfong, G.T. (Eds.), Autonomous Robot Vehicles. Springer New York, New York, NY, pp. 396–404. https://doi.org/10.1007/978-1-4613-8997-2_29.
Kim, S., Son, Y.-J., Chiu, Y.-C., Jeffers, M.A.B., Yang, C.Y.D., 2016. Impact of road environment on drivers' behaviors in dilemma zone: Application of agent-based simulation. Accid. Anal. Prev. 96, 329–340.
Kim, W., Zhang, J., Fujiwara, A., Jang, T.Y., Namgung, M., 2008. Analysis of stopping behavior at urban signalized intersections: empirical study in South Korea. Transp. Res. Rec. 2080 (1), 84–91.
Köll, H., Bader, M., Axhausen, K.W., 2004. Driver behaviour during flashing green before amber: a comparative study. Accid. Anal. Prev. 36 (2), 273–280.
Kometani, E., 1959. Dynamic behaviour of traffic with a nonlinear spacing-speed relationship. Theory of Traffic Flow 105–119.
Lee, D.N., 1976. A theory of visual control of braking based on information about time-to-collision. Perception 5 (4), 437–459.
Li, J., Zhang, H., Zhang, Y., Zhang, X., Dong, C., 2020. Modeling drivers' stopping behaviors during yellow intervals at intersections considering group heterogeneity. J. Adv. Transport. 2020, 1–11.
Li, M., Song, X., Cao, H., Wang, J., Huang, Y., Hu, C., Wang, H., 2019. Shared control with a novel dynamic authority allocation strategy based on game theory and driving safety field. Mech. Syst. Sig. Process. 124, 199–216.
Liu, H.X., Wu, X., Ma, W., Hu, H., 2009. Real-time queue length estimation for congested signalized intersections. Transp. Res. Part C 17 (4), 412–427.
Liu, T., Selpi, 2019. Comparison of car-following behavior in terms of safety indicators between China and Sweden. IEEE Trans. Intell. Transp. Syst. 21 (9), 3696–3705.
Long, K., Liu, Y., Han, L.D., 2013. Impact of countdown timer on driving maneuvers after the yellow onset at signalized intersections: An empirical study in Changsha, China. Saf. Sci. 54, 8–16.
Lu, G., Cheng, B.o., Lin, Q., Wang, Y., 2012. Quantitative indicator of homeostatic risk perception in car following. Saf. Sci. 50 (9), 1898–1905.
Lu, G., Cheng, B.o., Wang, Y., Lin, Q., 2013. A car-following model based on quantified homeostatic risk perception. Math. Probl. Eng. 2013, 1–13.
Lu, G., Wang, Y., Wu, X., Liu, H.X., 2015. Analysis of yellow-light running at signalized intersections using high-resolution traffic data. Transp. Res. Part A 73, 39–52.
Ma, Y., Qin, X., Grembek, O., Chen, Z., 2018. Developing a safety heatmap of uncontrolled intersections using both conflict probability and severity. Accid. Anal. Prev. 113, 303–316.
Mccrone, D.J., Arasteh, E., Jan, F.M., 2017. An artificial potential field approach to simulate cooperative adaptive cruise controlled vehicles. In: ASME 2017 Dynamic Systems & Control Conference. ASME, pp. 1-10.
Minderhoud, M.M., Bovy, P.H.L., 2001. Extended time-to-collision measures for road traffic safety assessment. Accid. Anal. Prev. 33 (1), 89–97.
Moore, D., Hurwitz, D.S., 2013. Fuzzy logic for improved dilemma zone identification: driving simulator study. Transp. Res. Rec. 2384 (1), 25–34.
Ni, D., 2013. A unified perspective on traffic flow theory, part I: the field theory. Appl. Math. Sci. 7, 1929–1946.
Papaioannou, P., 2007. Driver behavior, dilemma zone and safety effects at urban signalized intersections in Greece. Accid. Anal. Prev. 39 (1), 147–158.
Pathivada, B.K., Perumal, V., 2019. Analyzing dilemma driver behavior at signalized intersection under mixed traffic conditions. Transp. Res. Part F 60, 111–120.
Pawar, D.S., Pathak, D., Patil, G.R., 2020. Modeling dynamic distribution of dilemma zone at signalized intersections for developing world traffic. J. Transport. Saf. Secur. 14 (5), 886–904.

Rahman, M., Kang, M.-W., Biswas, P., 2021. Predicting time-varying, speed-varying dilemma zones using machine learning and continuous vehicle tracking. Transp. Res. Part C 130, 103310. https://doi.org/10.1016/j.trc.2021.103310.
Rakha, H., Amer, A., El-Shawarby, I., 2008. Modeling driver behavior within a signalized intersection approach decision-dilemma Zone. Transp. Res. Rec. 2069 (1), 16–25.
Rakha, H., El-Shawarby, I., Setti, J.R., 2007. Characterizing driver behavior on signalized intersection approaches at the onset of a yellow-phase trigger. IEEE Trans. Intell. Transp. Syst. 8 (4), 630–640.
Savolainen, P.T., 2016. Examining driver behavior at the onset of yellow in a traffic simulator environment: comparisons between random parameters and latent class logit models. Accid. Anal. Prev. 96, 300–307.
Setti, J.R., Rakha, H.A., El-Shawarby, I., 2007. Analysis of brake perception-reaction times on high-speed signalized intersection approaches. IEEE Intelligent Transportation Systems Conference. IEEE.
Sharma, A., Bullock, D., Peeta, S., 2011. Estimating dilemma zone hazard function at high speed isolated intersection. Transp. Res. Part C 19 (3), 400–412.
Tan, H., Lu, G., Liu, M., 2021. Risk field model of driving and its application in modeling car-following behavior. IEEE Trans. Intell. Transp. Syst. https://doi.org/10.1109/TITS.2021.3105518.
Tang, K., Xu, Y., Wang, F., Oguchi, T., 2016. Exploring stop-go decision zones at rural high-speed intersections with flashing green signal and insufficient yellow time in China. Accid. Anal. Prev. 95, 470–478.
Wang, J., Wu, J., Zheng, X., Ni, D., Li, K., 2016. Driving safety field theory modeling and its application in pre-collision warning system. Transp. Res. Part C 72, 306–324.
Wilde, G.J.S., 1982. The theory of risk homeostasis: implications for safety and health. Risk Anal. 2 (4), 209–225.
Wu, Y., Abdel-Aty, M., Ding, Y., Jia, B., Shi, Q., Yan, X., 2018. Comparison of proposed countermeasures for dilemma zone at signalized intersections based on cellular automata simulations. Accid. Anal. Prev. 116, 69–78.
Xiong, H., Narayanaswamy, P., Bao, S., Flannagan, C., Sayer, J., 2016. How do drivers behave during indecision zone maneuvers? Accid. Anal. Prev. 96, 274–279.
Yang, D., Ozbay, K., Xie, K., Yang, H., Zuo, F., Sha, D., 2021. Proactive safety monitoring: A functional approach to detect safety-related anomalies using unmanned aerial vehicle video data. Transp. Res. Part C 127, 103130.
Yang, M., Wang, X., Quddus, M., 2019. Examining lane change gap acceptance, duration and impact using naturalistic driving data. Transp. Res. Part C 104, 317–331.
Yang, Z., Tian, X., Wang, W., Zhou, X., Liang, H., 2014. Research on driver behavior in yellow interval at signalized intersections. Math. Probl. Eng. 1–8.
Yu, S., Shi, Z., 2014. An extended car-following model at signalized intersections. Phys. A. Stat. Mech. Appl. 407, 152–159.
Zhang, J., Tang, T., Wang, T., 2019. Some features of car-following behaviour in the vicinity of signalised intersection and how to model them. IET Intel. Transport Syst. 13 (11), 1686–1693.
Zhang, Y., Yan, X., Li, X., 2021. Effect of warning message on driver's stop/go decision and red-light-running behaviors under fog condition. Accid. Anal. Prev. 150, 105906.
Zhao, J., Kigen, K.K., Wang, M., 2020a. Modelling the operation of vehicles at signalised intersections with special width approach lane based on field data. IET Intel. Transport Syst. 14 (12), 1565–1572.
Zhao, X., He, R., Wang, J., 2020b. How do drivers respond to driving risk during car-following? risk-response driver model and its application in human-like longitudinal control. Accid. Anal. Prev. 148 (4), 105783.
Zhao, X., Li, Q., Xie, D., Bi, J., Lu, R., Li, C., 2018. Risk perception and the warning strategy based on microscopic driving state. Accid. Anal. Prev. 118, 154–165.
Zheng, X., Huang, H., Wang, J., Zhao, X., Xu, Q., 2021. Behavioral decision-making model of the intelligent vehicle based on driving risk assessment. Comput.-Aided Civ. Infrastruct. Eng. 36 (7), 820–837.
Zheng, Z., 2014. Recent developments and research needs in modeling lane changing. Transp. Res. Part B 60, 16–32.